Catalysis Today 150 (2010) 49–54

Contents lists available at ScienceDirect

Catalysis Today

journal homepage: www.elsevier.com/locate/cattod

Influence of the microstructure of carbon nanotubes on the oxidative dehydrogenation of ethylbenzene to styrene

J.J. Delgado [a,1], X. Chen [b], J.P. Tessonnier [a], M.E. Schuster [a], E. Del Rio [b], R. Schlögl [a], D.S. Su [a,*]

[a] Fritz-Haber-Institute of the Max Planck Society, Faradayweg 4-6, D-14195 Berlin, Germany
[b] Departamento de Ciencia de los Materiales e Ingeniería Metalúrgica y Química Inorgánica, Facultad de Ciencias, Universidad de Cádiz, E-11510 Puerto Real (Cádiz), Spain

ARTICLE INFO

Article history:
Available online 25 August 2009

Keywords:
Ethylbenzene
Styrene
Oxidative dehydrogenation
Carbon nanotube

ABSTRACT

The effect of graphitization of carbon nanotubes (CNTs) on the oxidative dehydrogenation of ethylbenzene to styrene was studied. An elimination of functional groups was observed by treating the catalyst under inert gas at temperatures below 1100 °C, while its microstructure and reactivity in TPO experiments did not change significantly. A decrease in the initial catalytic performances was observed, but the functional groups can be regenerated during the catalytic reaction, thus leading to a significant improvement in the catalytic activity. Annealing CNTs above 1500 °C leads to a well graphitisized wall structure of CNTs with a nearly oxygen-free surface with a low number of defects. The obtained samples show low but stable catalytic performances, indicating that the oxygenated active sites cannot be regenerated on this well-organized and low defective surface.

1. Introduction

Nanostructured carbon materials, especially carbon nanotube (CNT), have attracted the fancy of many scientists worldwide concerning their synthesis, properties, characterization and technological applications [1]. Among some of the most promising applications we can mention field emitter devices, drugs delivery and catalysis [1–7]. Carbon materials have been extensively used in catalysis not only as catalyst supports but also as highly active catalysts [8,9]. The new synthesis routes of nanostructured carbon materials allow to modulate their physical/chemical properties, opening new opportunities in the design of suitable catalysts for different reactions [10–13].

The oxidative dehydrogenation (ODH) of ethylbenzene to produce styrene has been proposed as a promising alternative to avoid the thermodynamic limitations, waste of energy and catalyst deactivation of the current industrial process [14]. Different carbon materials have been reported as active catalysts for the ODH reaction [15]. Activated carbon was proposed as a suitable catalyst for this reaction, but it exhibits a low and unstable activity in an oxidative atmosphere, hindering its use as industrial catalyst [16–18]. Carbon nanofilaments, tubes and onion-like carbon have also been reported to be active in the ODH of ethylbenzene to styrene and show high catalytic activity and stability [19]. The graphitic structure of CNTs and their low porosity compared with activated carbons are the main reason for their high stability under harsh operation condition. The nature and amount of basic groups, the crystallinity, textural properties and the ratio between the prismatic area and the basal plane area have been intensively studied in the literature to rationalise the catalytic performances of different carbon materials [20–24].

A redox mechanism involving quinone/hydroquinone groups presented on the carbon surface is suggested in the literature when activated carbon is used for the reaction [17]. A similar mechanism has been proposed for the CNTs where the basal planes exhibit metallic properties for oxygen activation, and nucleophilic Brønsted basic –C=O groups located at the edge/kink are the active sites for ethylbenzene dehydrogenation [19]. While the kinetics of the reaction and the influence of the pre-treatment of the nanocarbons on the reaction have been investigated [25], there is a lack of investigation on the effect of the graphitization degree on the intrinsic activity of CNTs, as well as on the active sites, their nature and stability during the reaction.

Here we report on the use of commercial CNTs with different graphitization degree as a model catalyst for the understanding of the structure–activity correlation in the ODH of ethylbenzene. The catalytic performance of the CNTs after different annealing pre-treatments gives us the role of the surface defects in the catalytic activity. The effect of the graphitization degree on the reaction rate and selectivity of ODH of ethylbenzene to styrene was studied. The surface and structural characterization of the fresh and used samples were investigated by TG–MS, XPS, TEM and EELS.

* Corresponding author. Tel.: +49 30 8413 5406; fax: +49 30 8413 4401.
E-mail addresses: juanjose.delgado@uca.es (J.J. Delgado), dangsheng@fhi-berlin.mpg.de (D.S. Su).
[1] Actual address: Departamento de Ciencia de los Materiales e Ingeniería Metalúrgica y Química Inorgánica, Facultad de Ciencias, Universidad de Cádiz, Spain.

0920-5861/$ – see front matter © 2009 Elsevier B.V. All rights reserved.
doi:10.1016/j.cattod.2009.07.103

Table 1
List of investigated carbon nanotubes and their main textural properties. Internal and external diameters were obtained by TEM (200 CNTs were counted). The oxygen content obtained by XPS and TPD integrations are also included.

Sample name	Annealing temperature (°C)	S_{BET} ($m^2\,g^{-1}$)	Average internal diameter (nm)[a]	Average external diameter (nm)[a]	Oxygen content before reaction (%)[b]	Oxygen content after reaction (%)[b]	Oxygen content after reaction ($\mu mol_O\,g_{cat}^{-1}$)[c]	EB conversion rate ($mmol\,g_{cat}^{-1}\,s^{-1}$)
CNT700	700	43 ± 4	43 ± 17	90 ± 31	3.1	12.9	5312.5	1.64
CNT950	950	39 ± 3	42 ± 18	92 ± 28	2.2	11.3	4772.9	1.34
CNT1100	1100	41 ± 4	43 ± 17	91 ± 32	0.8	7.0	2490.2	0.67
CNT1500	1500	32 ± 3	45 ± 21	93 ± 30	0.6	1.1	456.5	0.17
CNT3000	3000	34 ± 3	44 ± 18	96 ± 29	0.1	0.5	–	

[a] Calculated from TEM images.
[b] Calculated from XPS measurement.
[c] Calculated from oxygen elemental analysis.

2. Experimental

2.1. Catalyst

Commercial CNTs used in the present work were purchased from Pyrograf Products Inc. (OH, USA). They were synthesized by chemical vapor deposition (CVD) and subsequently heat-treated at 700, 1500 or 3000 °C by the provider (PR24-PS, PR24-LHT and PR24-HHT products, respectively). The commercial PR24-PS sample was post-treated under inert helium flow at different temperatures (950 and 1100 °C). A summary of the main results concerning the textural characterization of the samples is listed in Table 1.

2.2. Characterization techniques

Different bulk and surface sensitive techniques have been used to understand the catalytic properties of the samples. Transmission electron microscopy (TEM) analysis was performed with a Phillips CM200 FEG field-emission gun electron microscope operating at an accelerating voltage of 200 kV. The EEL spectra are representative of 20 aggregates distributed on the whole sample, while the electron beam has a width of approximately 400 nm. The XRD analysis was performed on a Bruker D8Advance diffractometer (Cu Kα radiation) with a scan step of 0.02° and a step time of 3 s. The nitrogen isotherms were measured at 77 K using a Micrometeritics ASAP 2010 system. The samples were outgassed for 2 h at 120 °C before the measurements. The surface area was calculated by using the Brunauer–Emmett–Teller (BET) method based on the adsorption data in the partial pressure (P/P_0) range 0.05–0.20.

X-ray photoelectron spectra were performed with a Kratos Axis Ultra DLD spectrometer employing a monochromated Al Kα X-ray source ($h\nu$ = 1486.6 eV). X-ray satellites and Shirley backgrounds were subtracted. The peak areas were normalized with the theoretical cross-sections to obtain the relative surface compositions.

The samples were also studied by temperature programmed oxidation (TPO). A flow of 60 $cm^3\,min^{-1}$ mixture of 20% O_2 in argon was used as an oxidant. The effluent gas was analysed by a mass spectrometer (Pfeiffer Thermostar instrument). In a typical experiment, about 2–4 mg of sample were loaded in a U shaped quartz reactor and the temperature was raised to 950 °C at a rate of 5 °C min^{-1}. Before the experiments, the samples were pre-treated under inert gas at 200 °C in order to eliminate the eventual adsorbed water.

The materials were further characterized by elemental analysis using a LECO CHNS-932 elemental analyser with a VTF 900 furnace for Oxygen Analysis.

2.3. Catalytic tests

The ODH of ethylbenzene to styrene reaction was carried out in a quartz tube reactor (8 mm i.d. × 300 mm) at 400 °C and at atmospheric pressure. 60 mg of catalyst particles (100–200 μm) was held between two quartz wool plugs in the isothermal zone. The reactant flow was a mixture of 2.7 vol.% EB and oxygen (O/EB ratio of 5:1) diluted in helium; the total space velocity is 5000 ml $g^{-1}\,h^{-1}$. No steam was added to the reactor. The analyses of the inlet and outlet gas were performed on an on-line gas chromatograph (Varian-3800) equipped with two columns for simultaneous analysis of aromatics and permanent gases: a 5% SP-1200/1.75% Bentone 34 packed column for the hydrocarbons and a Carboxen 1010 PLOT column for the permanent gases, coupled to FID and TCD detectors, respectively.

3. Results and discussion

Table 1 summarizes the textural characterization of the samples. All the samples have a similar surface area, which slightly decreases from 43 to 32 $m^2\,g^{-1}$ by increasing the annealing temperature. Only little differences in the inner and outer diameters of the CNTs can be observed between the samples, which is in good agreement with the BET measurements. Obviously, the specific surface area is related to the inner and outer diameters [26]. The low surface measured (around 40 $m^2\,g^{-1}$), in comparison with those obtained for SWCNT (up to 1200 $m^2\,g^{-1}$) can be easily explained by the large wall thickness (around 45 nm).

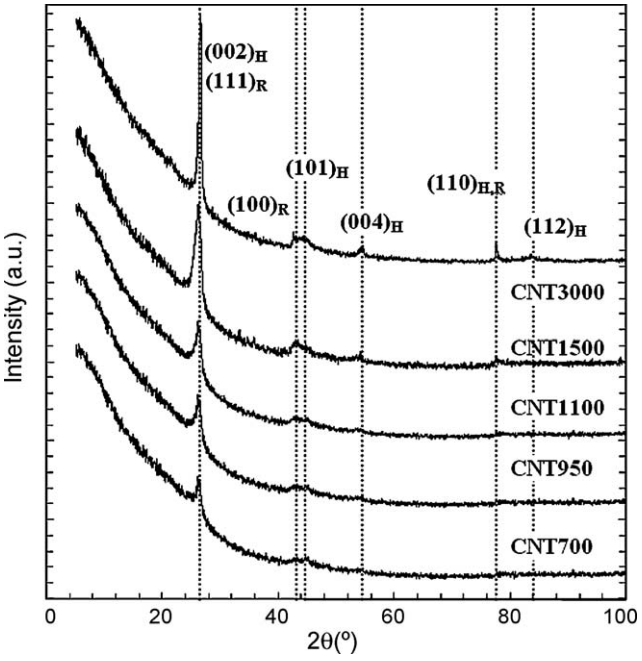

Fig. 1. XRD patterns of CNTs treated at different temperatures. The Miller index of the hexagonal and rhombohedral graphite is included and denoted by H and R subscript, respectively.

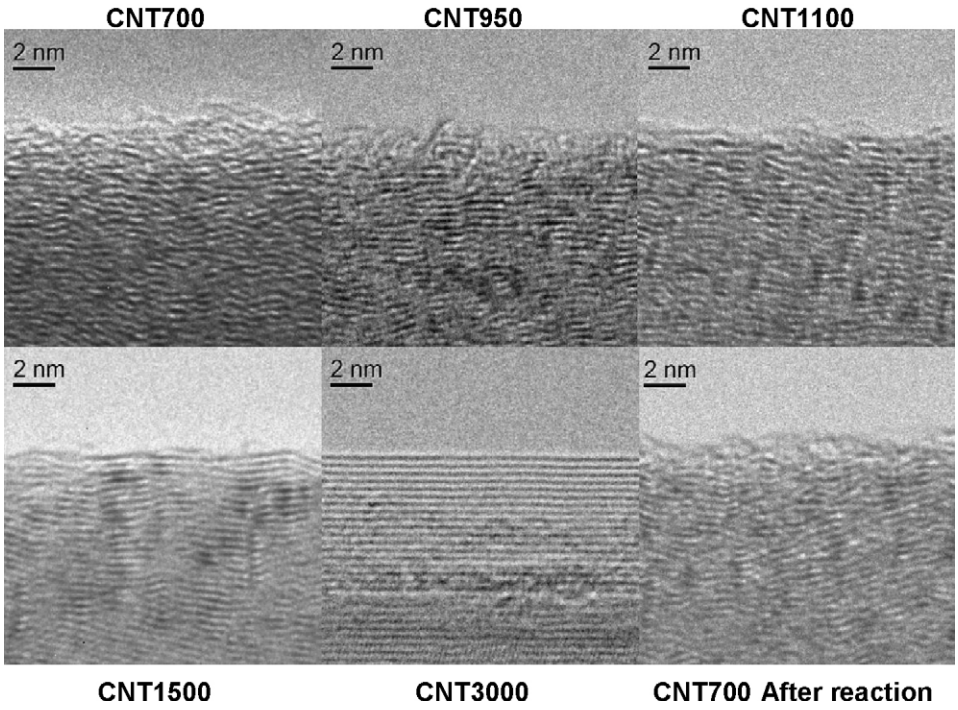

Fig. 2. High resolution TEM images of the CNTs treated at 700, 950, 1100, 1500 and 3000 °C. Image of sample CNT700 after reaction is also included.

X-ray diffraction was used to study the graphitic character and its effect on the catalytic performances. Even though the XRD pattern of CNTs can be explained using that of graphite, their interpretation can be complicated due to the turbostratic feature of CNT walls and the curvature. The size of the CNTs and their defective structure may induce peak broadening or eventually peak shift [27]. X-ray pattern of the studied samples is displayed in Fig. 1. Since all the samples have similar inner and outer diameters, any change in the diffraction pattern would be due to changes in the structural ordering. The diffraction patterns of the samples pre-treated below 1500 °C show a peak near 26° and a weak peak at 45°, which correspond to the strongest reflection either from hexagonal graphite (0 0 2) and (1 0 1) [28] or rhombohedral graphite (1 1 1) and (1 0 0) [29]. These peaks become sharper by treatment of the samples at higher temperature, indicating an increased graphitization degree of the samples. New diffraction peaks appear and become more obvious at 54°, 78° and 84° for the sample pre-treated at 3000 °C. The first and third peaks can only be attributed to hexagonal graphite, while the second may correspond to both hexagonal and rhombohedral graphite. However, the unexpected high value of the peak located at 78° may confirm the presence of rhombohedral graphite which coexists with the hexagonal structure.

HRTEM investigations of the samples confirm the results obtained by XRD. The initial disordered carbon structure is converted into a more and more ordered graphitic structure when raising the annealing temperature (Fig. 2). In the case of the sample CNT700, an ill carbonaceous structure is observed, even though it is not totally amorphous (Fig. 2). This structure is similar to low-temperature pyrolytic carbon deposited by CVD. No apparent difference can be found in the wall structure of the CNTs pre-treated up to 1100 °C (Fig. 2). Dramatic changes in the microstructure undergo by treating the sample at 1500 °C and higher temperature (Fig. 2). Long but greatly buckled graphene sheets are observed in the sample CNT1500. After annealing at 3000 °C, flat and almost perfectly ordered graphitic walls are observed (Fig. 2). Similar results have been reported by Mattia et al. for CNTs [30]. Oberlin reported similar steps for the graphitization process of a wide variety of carbon materials from cokes to carbon fibers [31]. The reorganization of the initial defective CNTs to a more graphitic material with well defined graphene sheets as revealed by XRD and imaged by HRTEM (Figs. 1 and 2) at temperatures above 1100 °C, i.e. when graphitization starts, is consistent with the progressive decrease in the surface area measured by nitrogen adsorption. The surface defects are active centers where the oxygenated species can be adsorbed. In principle, a higher number of defects can anchor a high number of oxygenated species. This is reflected in the high oxygen concentration of the samples CNT700, CNT900 and CNT1100, for which HRTEM in Fig. 2 reveals a higher structural disorder with more structural defects.

Fig. 3 shows the electron energy-loss near-edge fine structure (ELNES) spectra of the carbon K-edge for all the studied samples as well as the spectrum of a highly oriented pyrolytic graphite (HOPG)

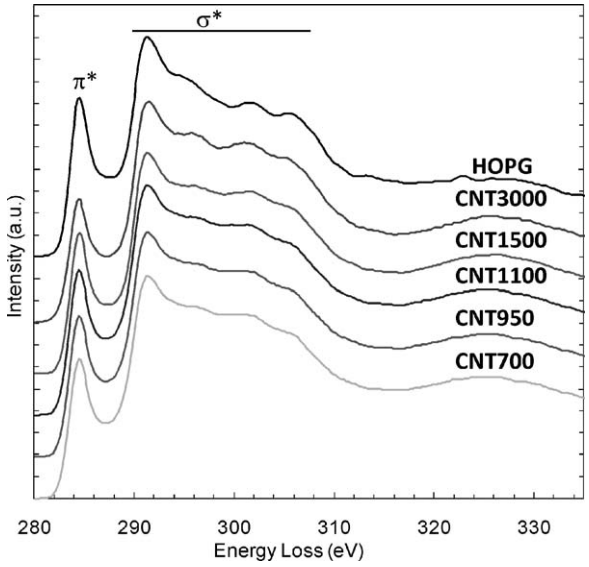

Fig. 3. EEL spectra of CNTs pre-treated at different temperatures. The spectrum of HOPG has been included for comparison.

as a reference. The ELNES spectra show a sharp peak around 285 eV which is related to the transition from the 1s to unoccupied states. This spectral feature is related with sp^2-hybridized carbon (i.e. graphite). The spectral features at 291–307 eV correspond to transitions from the 1s core shell to unoccupied σ^* states [32,33]. The π^* peak is more pronounced for the samples treated at higher temperature, indicating an increase of the sp^2 character (graphitization) in these samples. By raising the annealing temperature, the fine structure in the range of 293–308 eV becomes more defined. Those fine structures are also clearly observed in the HOPG spectrum, indicating the similarity in the structural order.

TPO was used to evaluate the stability of the sample under oxidizing conditions similar to the reaction condition, and to evaluate the density of defects on the catalyst surface. No big differences are observed in the CO_2 profile of the sample CNT700 and CNT950, although the peak becomes faintly narrower. A slight shift of the maximum gasification rate to higher temperatures is observed for the sample pre-treated at 1100 °C. For these three samples, XRD, TEM and EELS studies indicate the similar graphitization degree. This implies that the difference in the amount of surface structural defects causes the slight changes in the burning profile of these three samples. The samples treated at higher temperature have a lower concentration of oxygenated species on their surfaces [34,35]. A high on-set temperature for oxidation is then expected (Fig. 4).

More remarkable changes are observed in the TPO profiles of the samples treated at 1500 and 3000 °C, for which the gasification process occurs at higher temperature (700–750 °C). It is clear that the high graphitization degree of the samples increases their resistance towards combustion. A shift from a disordered structure to a more graphitic structure is accompanied by a rise in the temperature at which combustion takes place [34]. In fact, the microstructure of this sample revealed by TEM shows almost no structural defects. The lower combustion temperature observed for the samples pre-treated below 1500 °C may be explained by the presence of buckled graphene layers which introduce high structural tensions.

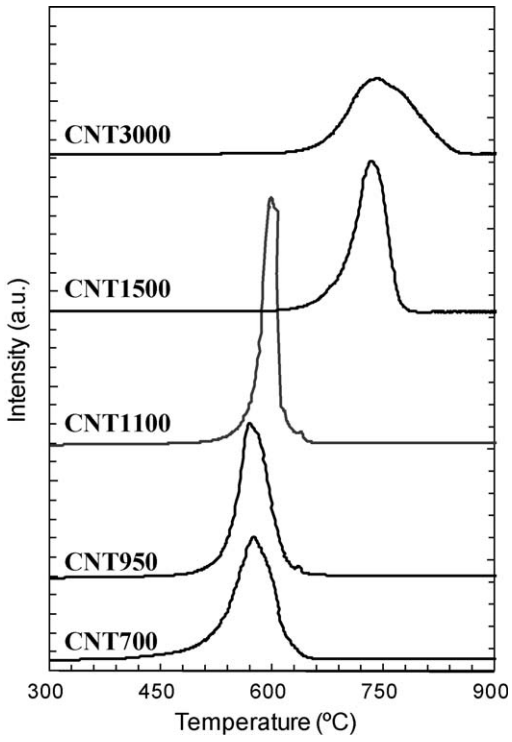

Fig. 4. CO_2 profiles of TPO experiments carried out using fresh catalysts.

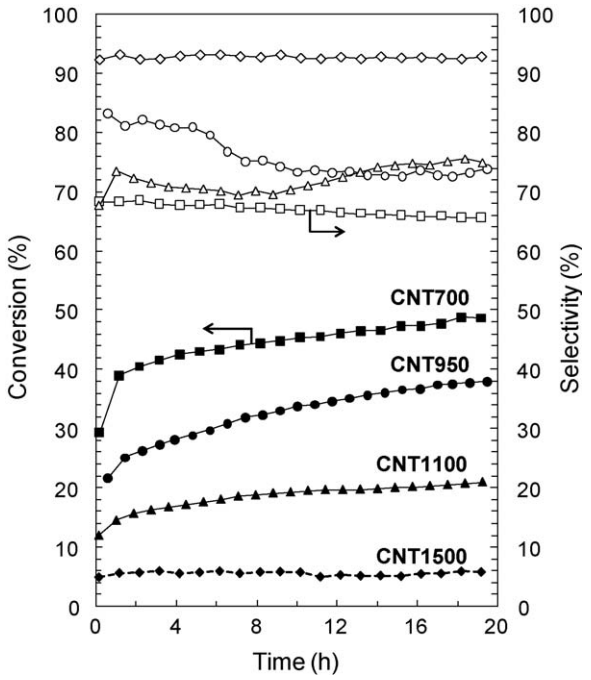

Fig. 5. Ethylbenzene conversion (filled symbols) and styrene selectivity (empty symbols) as a function of time on stream obtained at 823 K on CNTs previously treated at 700 °C (□), 950 °C (○), 1100 °C (△) and 1500 °C (◇).

The surface chemistry was evaluated in terms of the functional groups determined by XPS (Table 1). The concentration of functional groups on the samples treated above 1500 °C was found to be negligible (below 0.8%), while the maximum amount of oxygenated species (3.1%) was observed for the sample pre-treated at the lowest temperature (CNT700). The oxygen content decreases to 2.2% when increasing the annealing temperature up to 950 °C and becomes insignificant (0.8%) when the sample is treated at 1100 °C. These results are in line with the results obtained by TPO experiments and commented above.

The catalytic performances of the samples pre-treated at different temperatures are included in Fig. 5. The results obtained for the sample CNT3000 are not shown due to its negligible activity (<3%). We observe that the catalytic performances of the samples dramatically decrease with the annealing temperature, while the selectivity increases due to the low EB combustion observed, which leads to CO_2 formation (the only by-product observed). Another remarkable observation is that the catalytic activity increases during the reaction in the case of the samples pre-treated at temperatures below 1500 °C, while it is stable in the case of the samples treated at higher temperature. This transient activity period is more obvious in the case of samples CNT700 and CNT950, where a dramatic increase of 20% is observed in the catalytic activity. Different authors have pointed out the relationship between the catalytic activity and the presence of oxygenated groups on the catalyst surface [18,19,36]. In order to corroborate this assumption, the oxygen concentrations of the samples after reaction were measured by means of XPS and elemental analysis. The main changes in the amount of oxygen were observed for the samples annealed at temperatures below 1500 °C, where the oxygen content increases significantly after reaction. In fact, the oxygen content observed on the surface of the samples CNT700, CNT950 and CNT1100 was below 3.1% before reaction, while after reaction it was 12.9, 11.3 and 6%, respectively (Table 1). This is also in good concordance with the initial activation period, where these oxygenated groups were generated. The EB conversion rate is also included in Table 1 and it increases with the oxygen content

observed on the samples after reaction and obtained by XPS and elemental analysis.

Another remarkable observation is that the selectivity to styrene increases with the annealing temperature (Fig. 5). This phenomenon may have two possible explanations. Most likely, the increase in selectivity may have a kinetic origin in the lower overall reaction rate of ODH over high-temperature annealed CNT samples. A consecutive formation–combustion reaction network inevitably causes a decrease in ST selectivity with increasing reactant conversion. However, the styrene selectivity at different degrees of EB conversion should be compared to determinate the benefits of the microstructure on the reaction selectivity. The second possibility would be a structural change in the active sites during high-temperature treatment that lead to higher selectivity. As the selectivity (Fig. 5), in contrary to the conversion, does not follow a clear tendency, neither as a function of annealing temperature, nor as a function of time on stream, a certain impact of the nature of the active sites on styrene selectivity cannot be excluded.

Few impurities, in particular iron particles, were found in the samples treated at the lowest temperatures, between 700 and 1500 °C (see supporting information). However, the HRTEM investigation of these samples shows that the iron particles are always encapsulated. It is also remarkable that the HRTEM characterization of the samples after reaction corroborates that the iron particles are unaffected by the operation conditions and they remain encapsulated. This observation is also supported by XPS measurements of the fresh and used samples, as Fe was never detected in the survey spectra. Therefore, it is expected that the presence of iron in these samples does neither affect their catalytic activity nor their oxidation during TPO experiments.

Concerning the nature of the oxygenated groups present in the catalyst surface, the O 1s XP spectra (Fig. 6) can be deconvoluted using two peaks centered at 531.3 and 533.3 eV, which according to Xie and Sherwood [37] corresponds to quinoidic carbonyl groups (O_1, BE = 531.2–531.6 eV) and C–OH and/or C–O–C groups (O_2, BE = 533–534 eV). The contribution of each peak to the total oxygen signal was close to 50% (Table 2, supporting information). This fact hinders the possibility of studying the contribution of each functional group to the catalytic activity and determinate their role in the reaction mechanism. However, this is not in disagreement with the literature where it was reported that the quinoidic/carbonyl groups are responsible of the catalytic performance [18,19].

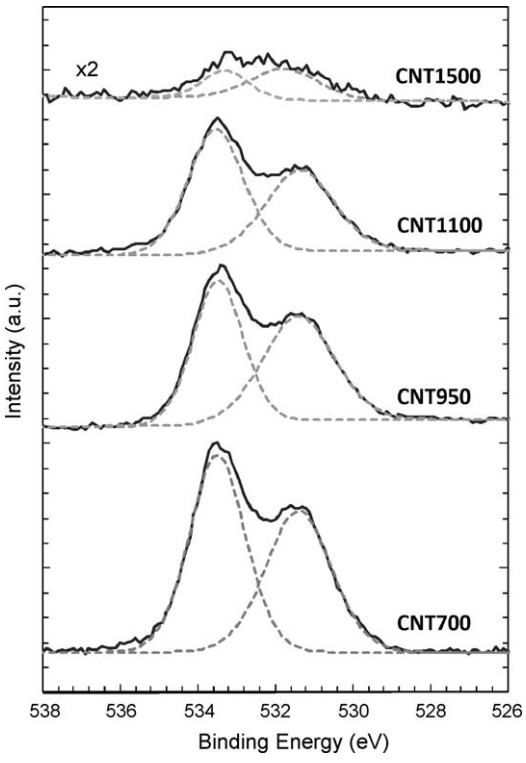

Fig. 6. XPS O1s spectra of the samples after reaction.

The catalytic tests as well as the TPO experiments confirm the high stability of the CNTs under oxidative conditions for temperatures below 450 °C. Indeed combustion is observed only above 450 °C. In addition, the catalytic activity measured at 400 °C is stable for 20 h on stream, which supports the absence of any deactivation due to combustion. TPO experiments however show that the combustion temperature decreases with the structural order, i.e. poorly ordered samples like CNT700 burn at a significantly lower temperature than well-ordered samples like CNT3000. Combustion, as well as the formation of oxygen-containing functional groups, takes place on structural defects, rich in sp^3 carbon atoms. O 1s XPS spectra confirm that the amount of surface oxygen-containing groups (Fig. 6) increases with the disorder in the CNT structure, and so with the density of defects. As a consequence, poorly ordered CNTs lead to higher EB conversions than well-ordered CNTs.

4. Conclusion

The present study indicates that the concentration of oxygenated functional groups on the catalyst surface is mainly responsible for the catalytic performance of the CNTs in ODH reactions. The samples treated at temperatures below 1100 °C exhibit a low initial catalytic activity, which significantly increases during the reaction time. This effect is due to the elimination of functional groups observed during the pre-treatment, and its regeneration during the reaction. The low and stable catalytic performances of the CNTs treated above 1500 °C can be easily explained if we consider their almost oxygen-free surface and low defected surface, which leads to low reactive surface like it was demonstrated from the TPO experiments.

Acknowledgements

J.J. Delgado and X. Chen thank financial support from the Ministry of Science and Innovation of Spain/FEDER Program of the EU (Project: MAT2008/00889NAN). The work in Berlin is preformed in the frame of EnerChem Project of Max-Planck-Society. The authors are grateful to Benjamin Frank for fruitful discussion.

Appendix A. Supplementary data

Supplementary data associated with this article can be found, in the online version, at doi:10.1016/j.cattod.2009.07.103.

References

[1] P. Ajayan, O. Zhou, in: M.S. Dresselhaus, P. Avouris (Eds.), Carbon Nanotubes Synthesis, Structure, Properties and Applications, Springer, Berlin/Heidelberg, 2001, p. 391.
[2] P. Serp, M. Corrias, P. Kalck, Appl. Catal. A 253 (2) (2003) 337.
[3] V. Sgobba, D.M. Guldi, Chem. Soc. Rev. 38 (2009) 165.
[4] Y.P. Sun, K. Fu, Y. Lin, W. Huang, Acc. Chem. Res. 35 (12) (2002) 1096.
[5] C. Klumpp, K. Kostarelos, M. Prato, A. Bianco, Biochim. Biophys. Acta Biomembr. 1758 (3) (2006) 404.
[6] H.G. Chae, S. Kumar, Science 319 (5865) (2008) 908.
[7] M.N. Tchoul, W.T. Ford, M.L.P. Ha, I. Chavez-Sumarriva, B.P. Grady, G. Lolli, D.E. Resasco, S. Arepalli, Chem. Mater. 20 (9) (2008) 3120.
[8] F. Rodríguez-Reinoso, Carbon 36 (3) (1998) 159.
[9] R. Schlögl, in: G. Ertl, H. Knözinger, F. Schüth, J. Weitkamp (Eds.), Handbook of Heterogeneous Catalysis, Wiley–VCH Verlag, 2007.
[10] L. Chen, K. Yang, H. Liu, X. Wang, Carbon 46 (15) (2008) 2137.

[11] X. Cui, J. Shi, L. Zhang, M. Ruan, J. Gao, Carbon 47 (1) (2009) 186.
[12] L. Gan, H. Du, B. Li, F. Kang, Carbon 46 (15) (2008) 2140.
[13] W. Chen, Z. Fan, X. Pan, X. Bao, J. Am. Chem. Soc. 130 (29) (2008) 9414.
[14] F. Cavani, F. Trifiro, Appl. Catal. A 133 (2) (1995) 219.
[15] J. Díaz Velásquez, L.M.C. Suarez, J.L. Figueiredo, Appl. Catal. A 311 (2006) 51.
[16] M.F.R. Pereira, J.J.M. Órfão, J.L. Figueiredo, Appl. Catal. A 218 (1–2) (2001) 307.
[17] M.F.R. Pereira, J.J.M. Órfão, J.L. Figueiredo, Appl. Catal. A 196 (1) (2000) 43.
[18] M.F.R. Pereira, J.J.M. Órfão, J.L. Figueiredo, Appl. Catal. A 184 (1) (1999) 153.
[19] D.S. Su, N. Maksimova, J.J. Delgado, N. Keller, G. Mestl, M.J. Ledoux, R. Schlogl, Catal. Today 102–103 (2005) 110.
[20] M.F. Pereira, J.L. Figueiredo, J.J.M. Órfão, P. Serp, P. Kalck, Y. Kihn, Carbon 42 (14) (2004) 2807.
[21] T.J. Zhao, W.Z. Sun, X.Y. Gu, M.M. Rønning, D. Chen, Y.C. Dai, W.K. Yuan, A. Holmen, Appl. Catal. A 323 (2007) 135.
[22] D. Su, N.I. Maksimova, G. Mestl, V.L. Kuznetsov, V. Keller, R. Schlögl, N. Keller, Carbon 45 (11) (2007) 2145.
[23] M.F.R. Pereira, J.J.M. Órfão, J.L. Figueiredo, Colloids Surf. A: Physicochem. Eng. Aspects 241 (1–3) (2004) 165.
[24] A. Guerrero-Ruiz, I. Rodríguez-Ramos, Carbon 32 (1) (1994) 23.
[25] J. Zhang, D.S. Su, A. Zhang, D. Wang, R. Schlögl, C. Hébert, Angew. Chem. Int. Ed. 46 (38) (2009) 7319.
[26] A. Peigney, C. Laurent, E. Flahaut, R.R. Bacsa, A. Rousset, Carbon 39 (4) (2001) 507.
[27] M. Abe, H. Kataura, H. Kira, T. Kodama, S. Suzuki, Y. Achiba, K.i. Kato, M. Takata, A. Fujiwara, K. Matsuda, Y. Maniwa, Phys. Rev. B 68 (4) (2003) 041405.
[28] P. Trucano, R. Chen, Nature 258 (5531) (1975) 136.
[29] H. Lipson, A.R. Stokes, Proc. Roy. Soc. Lond. A 181 (984) (1942) 101.
[30] D. Mattia, M.P. Rossi, B.M. Kim, G. Korneva, H.H. Bau, Y. Gogotsi, J. Phys. Chem. B 110 (20) (2006) 9850.
[31] A. Oberlin, Carbon 22 (6) (1984) 521.
[32] J. Yuan, L.M. Brown, Micron 31 (5) (2000) 515.
[33] K. Suenaga, E. Sandro, C. Colliex, C.J. Pickard, H. Kataura, S. Iijima, Phys. Rev. B 63 (16) (2001) 165408.
[34] M.R. Cuervo, E. Asedegbega-Nieto, E. Díaz, S. Ordóñez, A. Vega, A.B. Dongil, I. Rodriguez-Ramos, Carbon 46 (15) (2008) 2096.
[35] E. Díaz, S. Ordóñez, A. Vega, J. Colloids Interface Sci. 305 (1) (2007) 7.
[36] J.A. Garcia-Agulló, D. Cazorla-Amorós, A. Linares-Solano, U. Wild, D.S. Su, R. Schlögl, Catal. Today 102–103 (2005) 248.
[37] Y. Xie, P.M.A. Sherwood, Chem. Mater. 2 (3) (1990) 293.